Optimal Trajectory Study of a Small Size Waverider and Wing-Body Reentry Vehicle at Suborbital Entry Speed of Approximately 4 km/s with Dynamic Pressure and Heat Rate Constraint

S. Tauqeer ul Islam Rizvi[i*]; He Linshu[ii] and Tawfiqur Rahman[iii]

Received 26 Mar 2012; accepted 27 Oct 2012

ABSTRACT

A numerical trajectory optimization study of two types of lifting-entry reentry vehicle has been presented at low suborbital speed of 4.113 km/s and -15 degree entry angle. These orbital speeds are typical of medium range ballistic missile with ballistic range of approximately 2000 km at optimum burnout angle of approximately 41 degree for maximum ballistic range. A lifting reentry greatly enhances the reentry range which leads to a higher overall range of approximately 3000 km for the same ΔV. The optimum reentry angle of lifting reentry vehicle for medium range missiles under constrained g-load lies between -15 to -20 degree for limited g-load trajectories. These entry angles result in high decent rates and the vehicle quickly approaches the heat rate boundary. The heat rate problem is more severe for small size vehicle because of small nose-radius. Limiting the heat rate restricts the trajectory and lowers the downrange/cross-range performance of the reentry vehicle. A wing-body reentry vehicle has a larger nose radius as compared to a waverider which results in comparatively low heat rates during flight. This type of a vehicle has lower lift-to-drag ratio and therefore lesser range in comparison to a waverider type design. The performance of the two vehicle types is studied at various heat rate limits with the objective to calculate the optimum control deflections that would maximize the cross range. The results provide performance of the two designs vis-à-vis maximum heat rate constraint at the stagnation point along with the required control history. General pseudo-spectral optimal control software, GPOPS has been used for the optimal trajectory studies.

KEYWORDS

Trajectory Optimization, Optimal Control, Reentry Guidance, Lifting Reentry, Conceptual Design, Ballistic Missiles, Radau Pseudospectral Method

1. INTRODUCTION

The performance of a lifting entry vehicle is linked to the lift-to-drag ratio of the vehicle. In addition lifting reentry can also be used to attain the impact at the desired terminal flight path angle and speed. The higher cross range capability also give the end user a choice to select the missile trajectory and attack a target from different azimuth angles. High lift-to-drag ratio vehicles also perform a skipping maneuver within the atmosphere which makes interception by a chasing missile more demanding. The choice of terminal flight conditions, variable trajectories in combination with a skipping maneuver after reentry makes the choice of lifting reentry more attractive.

An integrated wave-rider has a lift-to-drag ratio close to 4 at Mach 4.0 [1] . Philips[2] has given a detailed overview of CAV-H and CAV-L concepts of Boeing wave rider designs and has also provided aerodynamic data which indicates a lift-to-drag ratio of greater than 3.0 at hypersonic mach number range for a typical high performance CAV design. This high aerodynamic performance is not without any limitation. The NASA

[i] Corresponding Author,S.T. Rizvi is a PhD Student in School of Astronautics, Beijing University of Aeronautics and Astronautics, 37-XueYuan Road, 100191 Beijing, China. (rizvi.aeng@gmail.com)

[ii] Professor He Linshu is faculty member in School of Astronautics, Beijing University of Aeronautics and Astronautics, 37-XueYuan Road, 100191 Beijing, China. (helinshu@sina.com)

[iii] T. Rahman is PhD Student in School of Astronautics, Beijing University of Aeronautics and Astronautics, 37-XueYuan Road, 100191 Beijing, China. (tawfiqurRahman@hotmail.com)

Ames and Sandia's Slender Aerodynamic Research Probe (SHARP L1) has a nose leading edge radius of the order of 3 millimeters[3] and therefore experiences very high heating rates during the reentry phase. The waverider technology is still undergoing test and trial in the form of X-41[4] vehicle by DARPA.

A wing-body vehicle has a lift-to-drag ratio close to 2.0. Whitmore[3] in his analysis has compared the data of shuttle, X-20 Dynasoar, X-34 and the X-15. The details of the MaRRV aerodynamic data are given by Parish-II [5] while Bornemann [6] and Surber [7] have presented the trim aerodynamic data of Shuttle Orbiter. The wing-body design is a compromise that allows for a spacecraft to perform a lifting reentry while still managing the extreme heat of reentry. In hypersonic flow blunt bodies tend to produce a strong detached normal shockwave at the nose. The detached shockwave causes a significant portion of the kinetic energy from a high-speed flow to be swept away by the cross-flow, so the majority of the energy never reaches the surface of the body.

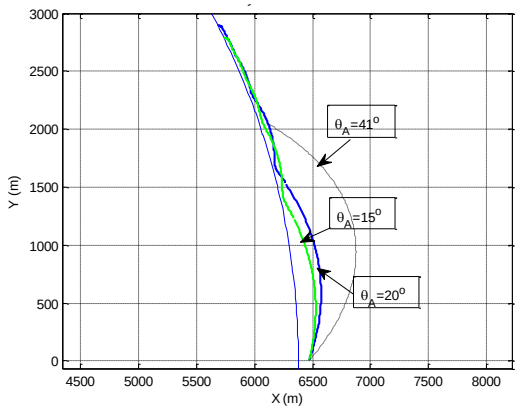

Figure 1: Trajectory comparison of a ballistic and lifting-body vehicle at burnout velocity of 4.113 km/s and different burnout angles.

The reentry studies performed in the past on wing-body configuration have focused mainly on manned reentry vehicles [8], Orbital Space Planes and reentry orbital transfer Vehicles [9, 10]. The waverider configuration type vehicles have been studied for Maneuvering Reentry Vehicles (MaRV) [5] for Intercontinental Ballistic Missiles application. These entire ranges of vehicles reenter the earth's atmosphere at low entry angles and at higher entry speeds. The optimum reentry angle of lifting reentry vehicle for medium range missiles lies between -15 to -20 degree for constrained g-load trajectories[11]. In Comparison with a ballistic trajectory, representative trajectories at entry speed of 4.113 km/s are shown in Fig. 1. It can be seen that ballistic plus reentry range of approximately 3000 km can be obtained for entry angle of -20 degree with a wing-body reentry vehicle and a total ΔV of 4.113 km/s which is 50% more than that of a pure ballistic trajectory. Typically sharp entry angles result in high decent rates and the vehicle quickly approaches the heat rate boundary. The heat rate problem is more severe for small size vehicle because of small nose-radius. Limiting the heat rate restricts the trajectory and lowers the downrange/cross-range performance of the reentry vehicle. In addition, the normal g-load required to perform the first skip is higher for sharper entry angles. Reducing burnout angle to less than 15 degree results in sharp decline, in over all range of the medium range ballistic missile [11].

The present study is aimed at computing waverider performance at reentry speed of 4.113 km/s which is typical of a medium range ballistic missile with ballistic range of approximately 2000 km. The results are compared with those of a wing-body configuration under varying heat rate constraint. The vehicle mass is assumed to be 1000 kg with 500 kg of payload mass. The wing-loading for both vehicles is assumed to be 400 kg/m^2 which is consistent with that of fighter aircrafts as well as MaRRV data considered in reference [9]. The vehicle data for the two types of vehicle under consideration and the physical constants are summarized in Table 1.

TABLE 1
VEHICLE DATA AND PHYSICAL CONSTANTS

Quantity	Numerical Values
Mass, kg	1000
W/S, kg/m^2	400
R_N, m *(lifting body)*	0.075
R_N, m *(waverider)*	0.003
r_e, m	6378 x 10^3
P_0, kg/m^3	1.225
M, m^3/s^2	3.986 x 10^{14}
B, m	7200

The study provides unconstraint (maximum) as well as near minimum heat load trajectory (minimum performance) for the waverider design. The latter results are compared with the wing-body trajectory corresponding to the same initial conditions. The results are critical for conceptual design studies in the later phase. The suitability of the configuration would depend upon the mass fraction of the TPS in a later design study. The trade-off studies are not part of the current paper.

2. PHYSICAL MODEL

A. Earth and Atmosphere

The earth has been assumed to be a perfect, non-rotating sphere. The acceleration due to gravity is given by Newton's inverse square law. The density variation with altitude is assumed to be exponential and given by the relation:

$$\rho = \rho_0 e^{(-h/\beta)} \quad (1)$$

where ρ_0 is the sea level density.

B. Aerodynamic Model

`The following set of equations represents the aerodynamic model of a wing-body vehicle. The trim aerodynamic data using references [5, 7, 8] has been used to obtain the following equations.

$$C_L = -0.034 + 0.93\alpha \quad (2)$$

$$C_D = 0.037 - 0.1\alpha + 0.736\alpha^2 + 0.937\alpha^3 \quad (3)$$

The aerodynamic model for the waverider configuration was obtained using the experimental data of the Crockrell [1]. The lift curve slope has been adjusted to that of a flat plate at hypersonic speeds obtained using Newtonian flow theory [12]. This is done since the data provided in reference [1] is only valid till Mach 4.5. The equations for a waverider configuration are:

$$C_L = -0.04 + 0.8\alpha \quad (4)$$

$$C_D = 0.012 - 0.1\alpha + 0.6\alpha^2 \quad (5)$$

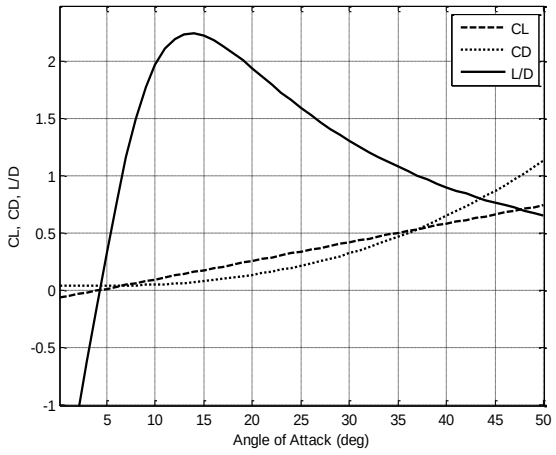

Figure 2: Lift-to-drag ratio variations with angle-of-attack for a wing-body configuration.

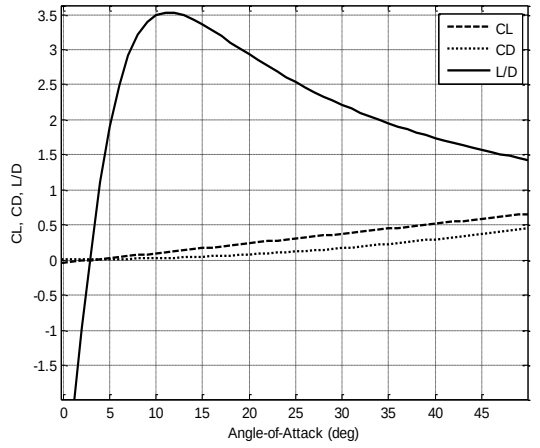

Figure 3: Lift-to-drag ratio variations with angle-of-attack for a waverider configuration.

C. Equations of Motion

The following set of equations of motion is used for a three- degree- of- freedom (DOF) point mass model. The equations have been extensively used in the study of reentry vehicle and their guidance systems [9, 10, 13].

$$\frac{dr}{dt} = V\sin\gamma \quad (6)$$

$$\frac{d\Theta}{dt} = \frac{V\cos\gamma\sin\psi}{r\cos\varphi} \quad (7)$$

$$\frac{d\Phi}{dt} = \frac{V\cos\gamma\cos\psi}{r} \quad (8)$$

$$\frac{dV}{dt} = -D - g\sin\gamma \quad (9)$$

$$\frac{d\gamma}{dt} = L\cos\sigma - \frac{\cos\gamma}{V}\left(g - \frac{V^2}{r}\right) \quad (10)$$

$$\frac{d\psi}{dt} = \frac{1}{V}\left[L\frac{\sin\sigma}{\cos\gamma} + \frac{V^2\cos\gamma\sin\psi\tan\phi}{r}\right] \quad (11)$$

where, r is the radial distance from the center of the earth to the reentry vehicle. Θ and φ are the longitude and latitude, respectively. V is the total velocity of the vehicle. γ and ψ are the flight path angle and the azimuth angle, respectively. The terms L and D are defined as L= $CL\rho V^2S/$ (2mass) and D= $CD\rho V^2S/$ (2mass). Thrust has been assumed to be zero during the entire flight. CL and CD are assumed to be only function of angle of attack. This is true in hypersonic region in which the aerodynamic coefficients do not vary with Mach number.

D. Stagnation Point Heat Rate

The stagnation point heating rate is modeled by using equation given by Scot et. al [14]. The convective heat transfer rate is given by:

$$\dot{Q} = \frac{18{,}300}{\sqrt{R_N}}\rho^{0.5}\left(\frac{V}{10^4}\right)^{3.05} \quad (12)$$

The equation is valid for a flow in chemical equilibrium. For non-catalytic hot walls (NCHW) the heat transfer rate is much lower because the molecules do not recombine at the skin surface. Zoby et al.[15] have computed the ratio of fully catalytic hot wall (FCHW) heat transfer rate to that of the non-catalytic hot wall (NCHW) heat transfer rate and have found that it is a function of the nose radius, R_N. For a nose radius of 0.075 m, the ratio of NCHW heat transfer rate to that of FCHW is approximately 50 percent to [16]. The heat transfer equation becomes:

$$\dot{Q} = \frac{1}{2}.\frac{18{,}300}{\sqrt{R_N}}\rho^{0.5}\left(\frac{V}{10^4}\right)^{3.05} \quad (13)$$

The total heat load at the stagnation point is calculated using the relationship:

$$Q = \int_{t_0}^{t_f} \dot{Q} dt \tag{14}$$

E. Normal Acceleration

For a winged body the normal acceleration is of greater importance as compared to the total deceleration load. The normal acceleration is computed using the relation given in equation (14).

$$n_z = \frac{L\cos\alpha + D\sin\alpha}{g} \tag{15}$$

where

$$g = \frac{\mu}{r^2} \tag{16}$$

F. Controls

The vehicle has angle-of-attack and bank-angle control. The vehicles are assumed to have angle-of-attack trim capability up from -10 - 50 degree angle of attack and a bank angle control of $\pm$ 90 degree. The angle-of-attack control modulates the lift as well as the heat rate. The bank angle results in lateral force which causes the sideward motion of the spacecraft.

3. BOUNDARY CONDITIONS AND CONSTRAINTS

A. Initial Conditions

The optimum Reentry velocities for maximum range of a ballistic missile are computed corresponding to a missile range of 2000 km using the relations given by He Linshu [17]. The optimum velocity for maximum range at the end of powered phase is given by the relationships:

$$V_A(f) = 11.19\sqrt{\tan(\frac{R_{B.F}}{222.4})\tan(45^0 - \frac{R_{B.F.}}{444.8})} \tag{17}$$

where, $R_{B.F.}$ is the ballistic flight range. It may be noted that the total range of the ballistic missile is given by the sum of powered flight, ballistic flight and the reentry range as:

$$R = R_A + R_{B.F.} + R_C \tag{18}$$

The optimum reentry angle for the maximum downrange/ cross-range has already been shown to lie in the range of 15-20 degree for a lifting reentry vehicle. It is because of this reason that the comparative performance between a waverider configuration and a lifting-body is performed at a reentry angle of 15 degree; this implies

$$V_0 = V_c(i) = V_A; \gamma_0 = \gamma_c(i) = -\theta_A = -15\text{deg} \tag{19}$$

V_A is calculated using Eq. (17) and the values are tabulated in Table 2. The Following set of initial conditions are used for the rest of the state variables:

$$r(i) = 6458\times10^3 m; \theta(i) = 0; \phi(i) = 0; \psi(i) = 0 \tag{20}$$

B. Terminal Conditions

For a maximum penetration of a conventional warhead, it is desirable that the warhead may be able to strike the target at maximum possible velocity and at a high impact angle close to 90 degree. For bi-conic reentry shapes the impact velocity is close to 700-1000 m/sec. Use of lifting reentry vehicles gives the military planners to strike a particular target at the desired angle and speed. Too high an impact speed improves the performance of the warhead alone but raises the maximum dynamic pressure limit of the reentry body. This implies a higher structural limit as well as a higher empty weight. For the current study, the maximum terminal speed is considered to be 720 m/s at an impact angle of 80 degree. The requirement has been modeled as a terminal constraint.

$$V(f) = 720 m/s; \gamma(f) = -80\text{deg} \tag{21}$$

C. Dynamic Pressure Constraint

A dynamic pressure limit corresponds to the maximum stagnation pressure which the vehicle structure can bear in the presence of high acceleration loads. The terminal constraints imply that the vehicle would sustain a dynamic pressure of approximately 320 KPa close to impact. The dynamic pressure constraint of 320 KPa has been imposed as a path constraint during the entire flight. The dynamic pressure constraint is kept equivalent to that of experienced by the vehicle in terminal phase.

$$q = \frac{1}{2}\rho V^2 < 320{,}000 \text{ Pa} \tag{22}$$

D. Heat Rate Constraint

The waverider performance is evaluated at an equivalent higher heat rates because of a smaller nose radius. The heat rate constraint as that of a wing-body, for a waverider configuration is computed using Eq. (13). The heat rate constraint used for wing-body analysis and that for a waverider configuration is tabulated in Table 2.

$$\dot{Q}_{eq(WR)} = \dot{Q}_{LB}\frac{\sqrt{R_{N(WB)}}}{\sqrt{R_{N(WR)}}} = 5\times\dot{Q}_{WB} \tag{23}$$

The heat rate constraint is directly linked with the surface temperature if the surface is assumed to be in radiative equilibrium with the surroundings.

$$\dot{Q} = \sigma\varepsilon_{th}(T_g{}^4 - T_w{}^4) \tag{24}$$

If Tg << Tw, we will have:

$$Tw = \left(\frac{\dot{Q}}{\sigma\varepsilon_{TH}}\right)^{\frac{1}{4}} \tag{25}$$

where σ is the Stefan-Boltzmann constant which is equal to 5.67 x10^{-8} W/(m^2.K^4), and Ɛ is the surface emissivity which is generally close to 0.8.

TABLE 2
INITIAL CONDITIONS AND HEAT RATE CONSTRAINTS

V_A (km/s)	Θ_c (deg)	$\dot{Q}_{(WB)}$ (MW/m^2)	$\dot{Q}_{eq\,(WR)}$ (MW/m^2)
4.113	-15	∞,1.5,1.0	∞, 7.5,*5.0*

Using Eq. (25), the heat rate limit of 1.0 and 1.5 MW/m^2 for wing-body configuration correspond to the stagnation point temperature limits of approximately 2170^{o}K and 2400^{o}K, respectively. Heat rate limits of 5 &7.5 MW/m^2 for waverider configuration correspond to surface temperature limits of 3240^{o}K and 3600^{o}K, respectively.

The carbon-carbon composite material can retain its properties till temperature of 2800^{o}C or 3073^{o}K[18]. The temperature corresponds to a heat rate limit of approximately 4.0 MW/m^2.

4. Objective Functions

The objective is to find the angle-of-attack and bank angle control deflections that would maximize the cross-range of the reentry vehicle. Maximizing cross range is similar to maximizing the latitude at final time t_f once the reentry takes place along the equatorial line. The problem is a Mayers problem and can be expressed as:

$$J = \min(-x_3(t_f)) \tag{26}$$

5. Method Used

The optimal control reentry problem is solved using GPOPS [19] version 4.0. GPOPS uses the Radau Pseudospectral Method (RPM) for solving optimal control problem. The RPM is an orthogonal collocation method where the collocation points are the Legendre-Gauss-Radau points. It is a Gaussian quadrature implicit integration scheme. It has been demonstrated to converge exponentially fast for problems whose solutions are smooth.

6. Results

Optimal trajectories were obtained for corresponding to entry speed of 4.113 km/s and entry angle of -15 degree subject to dynamic pressure constraint of 320,000 Pa and all heat load constraints listed in Table 2 except heat load constraint of 5MW/m^2 for waverider configuration. The numerical results are tabulated in Table 3. It can be seen from the results that the waverider configuration has more than twice the cross-range as compared to that of a wing-body design. The cross-range performance decreases with reducing heat rate limit. The wing-body vehicle also shows a reasonable performance but at an order of magnitude less than to the total heat load and 5 times less than the heat rate limit.

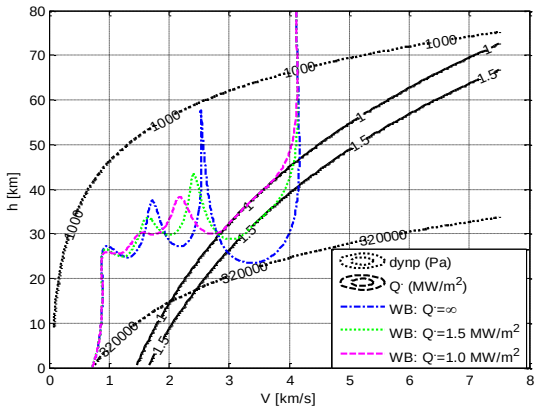

Figure 4: Altitude versus velocity plot for wing-body configuration with reentry velocity of 4.113 km/s and reentry angle of -15 degree.

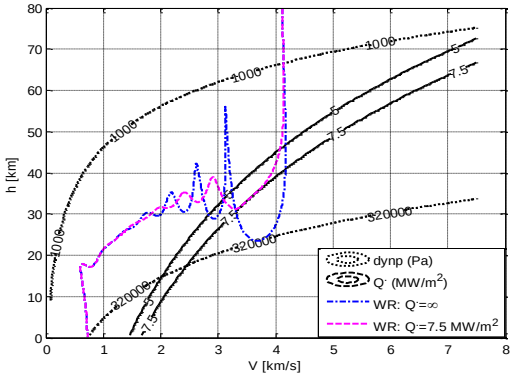

Figure 5: Altitude versus velocity plot for waverider configuration with reentry velocity of 4.113 km/s and reentry angle of -15 degree.

The trajectory shape for different heat rate constraints is presented in Figs. 4 & 5 for wing-body and waverider configurations, respectively. The figures clearly indicate that none of the flight path constraints is violated. The terminal constraints of velocity and flight path angle are also met. The heat rate and the dynamic pressure variations are given in Figs. 6 & 7. Reducing the heat rate limit drastically reduces the heat rate peak as well as the total flight time. Reduction in both these quantities results in lower integrated heat load.

Fig. 4 and Fig. 7 further indicate that for wing-body configuration heat rate constraint of 1 MW/m^2 is met for the wing-body vehicle approximately at an altitude of 45 km and speed of 3.8 km/s in the first 30 seconds of flight. The angle-of-attack control during the initial entry phase is used to modulate the lift as well as the heat rate. Fig. 8 shows that for a wing-body configuration the angle-of-attack saturates to a maximum of 50 degree at a reduced bank angle of -30 degree to ensure that the heat rate boundary of 1 MW/m^2 is not violated. This also results in a high drag which in turn results in both loss of energy and reduction range. Reducing the heat bound further does not result in a viable solution because of non-availability of additional control power. For a heat rate

boundary of 1.5 MW/m^2 the angle-of-attack goes to a maximum of 35 degree. The energy loss to drag force is comparatively less and this results in a higher range as compared to a 1.0 MW/m^2 boundary. For an unconstraint heat load boundary the cross-range performance is maximized but the heat rate peaks to more than 3.0 MW/m^2 and the total heat load increases to 0.21 x 10^9 J/m^2.

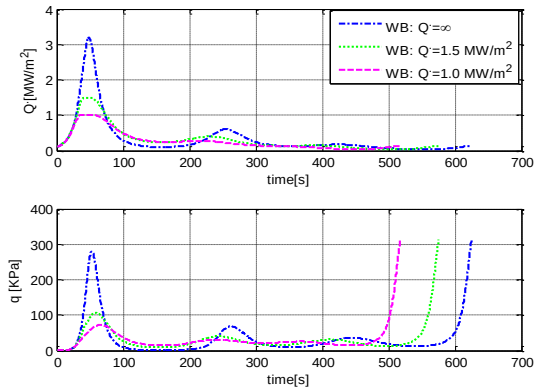

Figure 6: Heat rate and dynamic pressure variation with time for wing-body configuration at reentry speed of 4.113 km/s and -15 deg reentry angle.

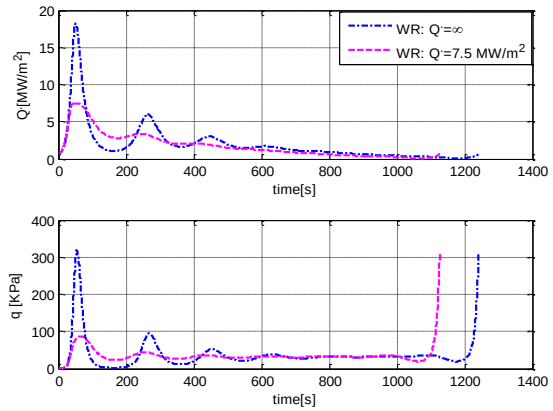

Figure 7: Heat rate and dynamic pressure variation with time for waverider configuration at reentry speed of 4.113 km/s and -15 deg reentry angle.

For a waverider configuration, Fig 9 indicates that the angle-of-attack control saturates to a maximum of 50 degree ensuring compliance with a heat rate limit of 7.5 MW/m^2. Reducing the heat rate bound does not result in a viable solution because the drag force cannot be further increased by increasing the angle-of-attack and further energy cannot be dissipated in the form of heat. The lift force is also not sufficient enough to initiate the first skip at a higher altitude and ensuring a lower heat limit. It can be further observed that for a near minimum heat rate bound of 7.5 MW/m^2 for a waverider configuration, the total heat load is approximately 2.0 x 10^9 J/m^2 which is 10 times more than the integrated heat load for a wing-body configuration unbounded heat rate trajectory. The integrated heat loads as well as the maximum normal loads for all optimal paths are tabulated in table 3. For waverider configuration with no heat rate constraint the maximum angle-of-attack goes to a value of 18 degree. In this case the limiting bound is not the heat rate limit but the dynamic pressure limit of 320,000 Pa (Fig. 3 & 7).

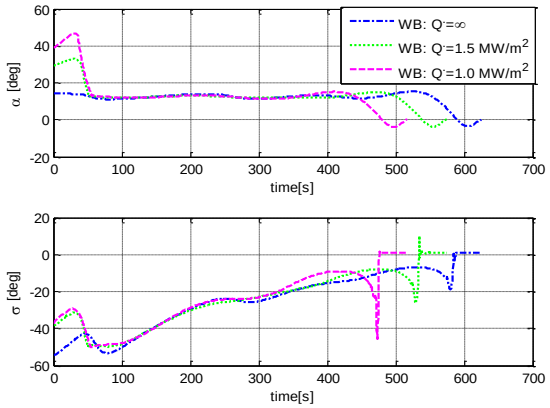

Figure 8: Flight controls deflection with time for a wing-body configuration at reentry speed of 4.113 km/s and -15 degree reentry angle.

Both types of vehicles trim to an angle-of-attack of 12 degree during the mid-course phase (Fig. 10 & 11). The angle-of-attack corresponds to angle-of-attack at which lift-to-drag ratio peeks to maximum. This ensures minimum energy loss and maximum range. For waverider configuration the speed bleeds slowly due to of a lower drag which results in a higher range. At higher heat rate limits both vehicle execute a skipping type of trajectory. The constraint trajectories show diminishing skipping behavior with lowering a heat rate constraint and the trajectory comes closer to an equilibrium glide condition for a minimum value of heat rate constraint.

TABLE 3
NUMERICAL RESULTS FOR WING-BODY AND WAVERIDER CONFIGURATIONS

Geometry	V_A (km/s)	Θ_A (deg)	$\dot{Q}$ (MW/m^2)	T (s)	R_{down} (km)	R_{cross} (km)	n_{zmax} (g)	Q_{total} (GJ/m^2)
WB	4.113	15	∞	624.8	795.5	799.8	13.6	0.209
			1.5	575.1	752.0	665.6	9.2	0.178
			1.0	517.4	668.8	543.9	8.9	0.142
WR	4.113	15	∞	1241.2	1179.7	1948.3	12.2	2.436
			7.5	1126.5	1077.3	1590.0	8.9	2.001

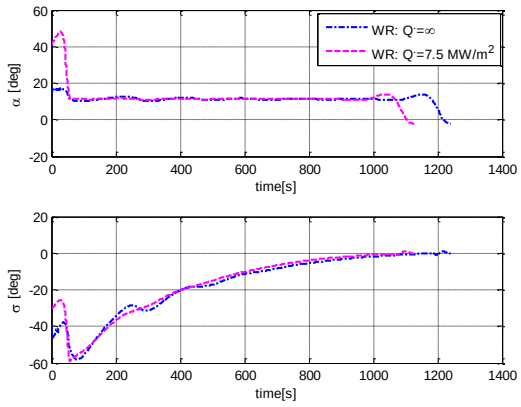

Figure 9: Flight controls deflection with time for wing-body configuration at reentry speed of 4.113 km/s and -15 degree reentry angle.

It can also be observed from Figs. 6, 7, 10 and 11 that the peak dynamic pressure, heat load as well as the normal acceleration are encountered at almost the same instant. The vehicle is also close to maximum bank angle at this instant. All these conditions together make the instant a critical design point in the whole trajectory.

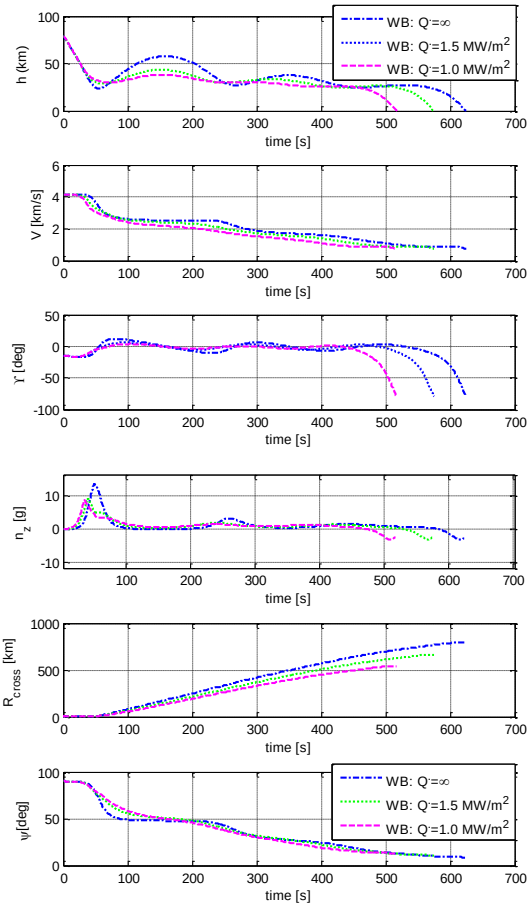

Figure 10: Flight parameters variation with time for wing-body configuration at reentry speed of 4.113 km/s and reentry angle of -15 degree.

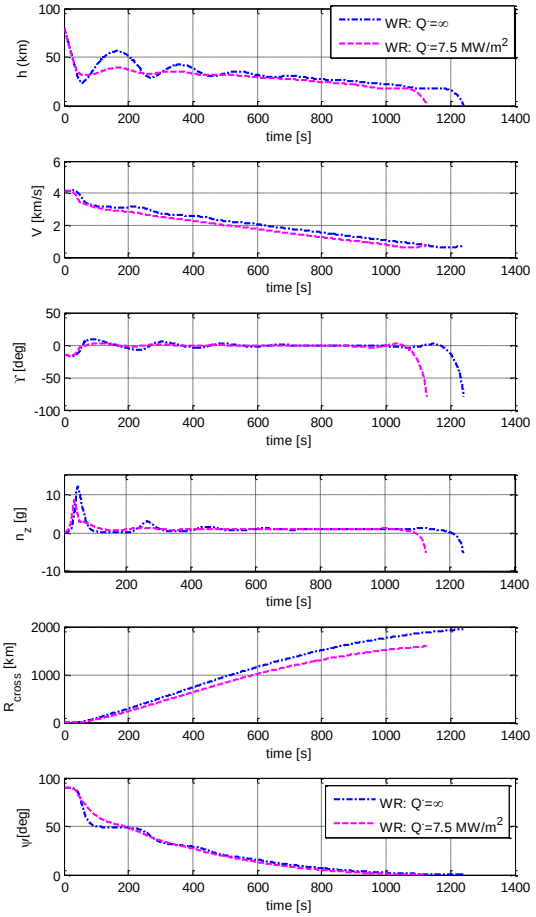

Figure 11: Flight parameters variation with time for waveride configuration at reentry speed of 4.113 km/s and reentry angle of -15 degree.

During the terminal phase both type of vehicles trim to negative angle-of-attack to dive down and meet the terminal angle and flight path constraint. Negative g-load from -3 to -5 g is experienced by the vehicle during this phase.

7. CONCLUSION

A trajectory analysis for a waverider and a wing-body configuration has been presented for entry condition of 4.113 km/s and reentry angle of -15 degree under unconstraint and constraint heat rate limits. The angle-of-attack and bank angle behavior time histories have been thoroughly discussed and related with flight paths as well as the constraints for both the lifting-body the waverider configuration. The waverider configuration has a higher performance as compared to a wing-body configuration. However, the waverider configuration can only perform at heat limit of 7.5 MW/m^2 and higher. The near minimum heat rate limit of 7.5 MW/m^2 is much higher than the upper limit of 4.0 MW/m^2 for carbon-carbon composite material. The wing-body design is the only possible option at ≈4 km/s reentry speed and -15 degree entry angle with the material limit.

8. REFERENCES

[1] C. E. Crockrell, L. D. Huebner, and D. B. Finley, "Aerodynamic Performance and Flow Field Characteristics of two wave-rider Derived Hypersonic Cruise Vehicles " in *AIAA 33rd Aerospace Science Meeting and Exhibit* Reno, NV: AIAA Paper 95-0736, 1995.

[2] T. H. Phillips, "A Common Aero Vehicle (CAV) Model, Description, and Employment Guide," Schafer Corporation for AFRL & AFSPC 2003.

[3] S. A. Whitmore and B. J. Dunbar, "Orbital Space Plane: Past, Present, and Future," in *IAA/ ICAS International Air and Space Symposium and Exposition*, Dayton, Ohio, 2003.

[4] "X-41 Common Aero Vehicle," GlobalSecurity.org, 2010.

[5] M. S. Parish-II, "Optmality of Aeroassisted Orbital Plane Changes," in *Naval Postgraduate School*. vol. Maters of Science Thesis Monterey, CA, 1995, p. 110.

[6] W. E. Bornemann and T. E. Surber, "Aerodynamic Design of the Space Shuttle Orbiter."

[7] T. E. Surber and D. C. Oslen, "Shuttle Orbiter Aerodynamic Development," *Journal of Spacecraft*, vol. 15, pp. 40-47, 1978.

[8] S. A. Whitmore, Daniel W. Banks, B. M. Andersen, and P. R. Jolley, "Driect-Entry, Aerobraking, and Lifting Aerocapture for Human Rated Lunar Return Vehicles," in *44th AIAA Aerospace Science Meeting and Exhibit*, Reno, Nevada, 2006, p. 29.

[9] F. Zimmermann and A. J. Calise, "Numerical Optimization Study of Aeroassisted Orbital Transfer," *Journal of Guidance Control and Dynamics*, vol. 21, pp. 127-133, January-Feburary 1998.

[10] D. G. Hull and J. L. Speyer, "Optimal reentry and Plane Change Trajectories," *The Journal of Astronautical Sciences*, vol. 30, pp. 117-130, 1982.

[11] S. T. Rizvi and L. He, "Optimal Performance Study of Wing-Body Reentry Vehicle for Medium to Intermediate Range Ballistic Missile Applications," Beijing University of Aeronautics and Astronautics, Beijing, China., 2012.

[12] J. John D. Anderson, "Hypersonic and High Temperature Gas Dynamics," in *Hypersonic and High Temperature Gas Dynamics*: McGraw-Hill Book Company, 1989, pp. 291-292.

[13] J. A. Love and L. W. Neustadt, "A simple re-entry guidance system," *Guidance and Control*, p. 49, 1963.

[14] C. D. Scot, R. C. Ried, R. J. Maraia, C. P. Li, and S. M. Derri, "An AOTV Aeroheating and Thermal Protection Study," in *Thermal Design of Aeroassisted Orbital Transfer Vehicles*. vol. 96, F. Nelson, Ed. New York: AIAA, 1985.

[15] E. V. Zoby, K. P. Lee, R. N. Gupta, and R. A. Thompson, "Nonequilibrium Viscous Shock Layers Solutions for Hypersonic Flow Over Slender Bodies," in *Eighth National Aero- Space Plane Technology Symposium*, Monterey, CA, Mar, 1990.

[16] J. J. Bertin, "Hypersonic Aerothermodynamics," in *Hypersonic Aerothermodynamics* Washington, DC: AIAA Education Series, 1994, pp. 257-262.

[17] "Launch Vehicle Design," H. Linshu, Ed.: BUAA Press, 2004, pp. 80-87.

[18] C. L. Darby and A. V. Rao, "Minimum-Fuel Low-Earth-Orbit Aeroassisted Orbital Transfer of Small Spacecraft," *Journal of Spacecraft and Rockets*, vol. 48, Jul.-Aug., 2011.

[19] A. V. Rao, "User's Manual for GPOPS Version 4.0," August, 2011.